HHS Public Access

Author manuscript

Cancer Res. Author manuscript; available in PMC 2019 March 27.

Published in final edited form as:

Cancer Res. 2018 March 01; 78(5): 1225–1240. doi:10.1158/0008-5472.CAN-17-1089.

The CARMA3-Bcl10-MALT1 Signalosome Drives NF-κB Activation and Promotes Aggressiveness in Angiotensin II Receptor-positive Breast Cancer.

Prasanna Ekambaram[1], **Jia-Ying (Lloyd) Lee**[1], **Nathaniel E. Hubel**[1], **Dong Hu**[1], **Saigopalakrishna Yerneni**[2], **Phil G. Campbell**[2,3], **Netanya Pollock**[1], **Linda R. Klei**[1], **Vincent J. Concel**[1], **Phillip C. Delekta**[4], **Arul M. Chinnaiyan**[4], **Scott A. Tomlins**[4], **Daniel R. Rhodes**[4], **Nolan Priedigkeit**[5,6], **Adrian V. Lee**[5,6], **Steffi Oesterreich**[5,6], **Linda M. McAllister-Lucas**[1,*], and **Peter C. Lucas**[1,*]

[1]Departments of Pathology and Pediatrics, University of Pittsburgh School of Medicine, Pittsburgh, Pennsylvania

[2]Department of Biomedical Engineering, Carnegie Mellon University, Pittsburgh, Pennsylvania

[3]McGowan Institute for Regenerative Medicine, University of Pittsburgh, Pittsburgh, Pennsylvania

[4]Department of Pathology, University of Michigan Medical School, Ann Arbor, Michigan

[5]Women's Cancer Research Center, Magee-Womens Research Institute, University of Pittsburgh Cancer Institute, Pittsburgh, Pennsylvania

[6]Department of Pharmacology and Chemical Biology, University of Pittsburgh School of Medicine, Pittsburgh, Pennsylvania

Abstract

The angiotensin II receptor AGTR1, which mediates vasoconstrictive and inflammatory signaling in vascular disease, is overexpressed aberrantly in some breast cancers. In this study, we established the significance of an AGTR1-responsive NF-κB signaling pathway in this breast cancer subset. We documented that AGTR1 overexpression occurred in the luminal A and B subtypes of breast cancer, was mutually exclusive of HER2 expression, and correlated with aggressive features that include increased lymph node metastasis, reduced responsiveness to neoadjuvant therapy, and reduced overall survival. Mechanistically, AGTR1 overexpression directed both ligand-independent and ligand-dependent activation of NF-κB, mediated by a signaling pathway that requires the triad of CARMA3, Bcl10, and MALT1 (CBM signalosome).

[*]**Corresponding Authors:** Peter C. Lucas, 5123 Rangos Research Building, Children's Hospital of Pittsburgh, University of Pittsburgh School of Medicine, 4401 Penn Avenue, Pittsburgh, PA 15224. Phone: 412-692-7608; Fax: 412-692-7816; lucaspc@upmc.edu and Linda M. McAllister Lucas, Phone: 412-692-7608; linda.mcallister@chp.edu.
Current address for P.C. Delekta: Department of Microbiology & Molecular Genetics, Michigan State University, East Lansing, Michigan
Current address for D.R. Rhodes: Strata Oncology, Ann Arbor, MI

Disclosure of Potential Conflicts of Interest:
S.A. Tomlins is a consultant for and receives honoraria from Roche/Ventana Medical Systems, Almac Diagnostics, Jansenn, AbbVie, Astellas/Medivation and Sanofi. S.A. Tomlins has sponsored research agreements with Compendia Biosciences/Life Technologies/ThermoFisher Scientific, Astellas and GenomeDX. D.R. Rhodes and S.A. Tomlins are Co-founders and equity holders in Strata Oncology. A.M. Chinnaiyan and D.R. Rhodes were Co-founders of Compendia Biosciences.
No potential conflicts of interest were disclosed by the other authors.

Activation of this pathway drove cancer cell-intrinsic responses that include proliferation, migration and invasion. In addition, CBM-dependent activation of NF-κB elicited cancer cell-extrinsic effects, impacting endothelial cells of the tumor microenvironment to promote tumor angiogenesis. CBM/NF-κB signaling in AGTR1+ breast cancer therefore conspires to promote aggressive behavior through pleiotropic effects. Overall, our results point to the prognostic and therapeutic value of identifying AGTR1 overexpression in a subset of HER2-negative breast cancers, and they provide a mechanistic rationale to explore the repurposing of drugs that target angiotensin II-dependent NF-κB signaling pathways to improve the treatment of this breast cancer subset.

PRECIS:

Findings offer a mechanistic rationale to explore the repurposing of drugs that target angiotensin action to improve the treatment of AGTR1-expressing breast cancers.

Keywords

Angiotensin; invasion; angiogenesis; breast carcinoma; Bcl10; MALT1

INTRODUCTION

While significant strides have been made in the treatment of breast cancer resulting in a decline in mortality over the past two decades (1), progress has been incomplete, and the medical armamentarium for treating this disease still relies heavily on non-specific, cytotoxic chemotherapeutics. Changing this scenario necessitates the development of more innovative and targeted therapies based on an increasingly nuanced understanding of breast cancer subtypes and their molecular drivers. One of the most significant advances in this regard has been in the development of therapeutic antibodies against ERBB2 (HER2), which drives 20–25% of breast cancers (2). However, most breast cancers (~75%) progress independently of HER2, so there remains a pressing need to discover the molecular determinants for these cancers, thereby uncovering new therapeutic targets for the next era of personalized medicine. This is particularly applicable to triple negative breast cancers, for which there is no targeted therapy, and for Luminal B cancers that may behave aggressively and prove resistant to hormonal therapy, despite their expression of estrogen receptor (ER) (3, 4).

Several years ago, we collaborated in a multidisciplinary effort to identify new receptors that might drive oncogenic progression in unique subsets of breast cancer (5). Using a bioinformatics approach termed Meta-Cancer Outlier Profile Analysis (MetaCOPA), we sought to nominate candidate oncogenes from multiple independent breast cancer profiling datasets, based on aberrantly high expression. We analyzed 31 published datasets comprising nearly 3,200 independent microarray experiments and found that the second most consistently high-scoring gene (after *HER2*) is *AGTR1*, which encodes the Angiotensin II type I receptor. AGTR1 is a member of the G protein-coupled receptor (GPCR) superfamily and is best known for its role in vascular biology (6, 7). Based on MetaCOPA analyses, we estimated that AGTR1 overexpression occurs in 15–20% of breast

cancers, and found that AGTR1 and HER2 overexpression define mutually exclusive subsets of disease.

Despite the identification of AGTR1 as a potential pathogenic driver in a subset of breast cancers, little is known regarding the mechanisms by which AGTR1 might affect signaling in breast cancer cells, or the phenotypic consequences of its overexpression. AGTR1 is capable of engaging a number of signaling pathways in vascular endothelial and smooth muscle cells, some of the cell types where it has been best studied (6, 8). As a result, it seems likely that AGTR1 overexpression coopts several pathways for aberrant activation in breast cancer. Indeed, Oh *et al* have clearly shown both aberrant ERK and SMAD3/4 activity in MCF7 breast cancer cells engineered to overexpress AGTR1 (9).

With the current work, we utilized newer profiling databases, including The Cancer Genome Atlas (TCGA) and METABRIC, to further interrogate *AGTR1* as an oncogene in breast cancer. In addition, we sought to explore the hypothesis that AGTR1 might mimic the actions of HER2 with regard to activation of NF-κB, one of the major downstream mediators driving pathogenesis of HER2+ breast cancer. This hypothesis was particularly compelling since AGTR1 and HER2 overexpression are mutually exclusive in breast cancer (5), suggesting that the two receptors direct redundant pathways as a means of promoting tumor progression. In support of this hypothesis, we find that AGTR1 harnesses a unique signaling pathway for activation of NF-κB, which involves assembly of the CARMA-Bcl10-MALT1 signalosome, best known as a critical regulator of immune responses in lymphocytes (10, 11). In breast cancer cells, AGTR1-dependent activation of this NF-κB pathway initiates a distinct set of responses, causing cells to adopt a proliferative, migratory, invasive, and pro-angiogenic phenotype.

AGTR1 has long been successfully targeted in the practice of cardiology by therapeutics that include both receptor antagonists [Angiotensin Receptor Blockers (ARBs) such as losartan] and inhibitors of ligand production [Angiotensin Converting Enzyme inhibitors (ACE inhibitors) such as captopril] (12). In addition, novel inhibitors of MALT1 are now being described, including some that have a history of use in psychiatric disorders (eg, the phenothiazines, mepazine and thioridazine) (13, 14). As a result, there exists an opportunity to explore repurposing of these legacy drugs in the novel arena of breast cancer therapy, provided we appropriately identify and select breast cancer patients with AGTR1 overexpression who might benefit from this combination therapy. The work described here provides preclinical validation for this concept and motivation to pursue this goal.

MATERIALS AND METHODS

Antibodies, Plasmids, and other Reagents

A detailed description of reagents and their sources can be found in the Supplementary Methods.

Cell lines and cell culture

BT549, HCC1500, ZR75–1, Hs578T, Hs606T, CRL-7548 and MDA-MB231 cells were obtained directly from ATCC, with cell line identities confirmed by short tandem repeat

(STR) profiling by the source. Frozen aliquots of cells were prepared upon receipt and all cell lines were passaged for less than 6 months. SKBR3 cells were kindly provided by Dr. Ira Bergman (Department of Pediatrics, University of Pittsburgh) and the identity of this line was authenticated by STR profiling at the University of Arizona Genetics Core (UAGC, Tucson, AZ). Primary HUVEC cells were obtained from Lonza and were maintained in culture for no more than 7 passages. BT549, HCC1500, ZR75–1 and SKBR3 cells were grown in Phenol Red Free RPMI-1640 media (Cat No: 11835030, Gibco, Waltham, MA) whereas MDA-MB231 were grown in DMEM-Glutamax media, both supplemented with 10% FBS, 1% penicillin/streptomycin (Gibco, Waltham, MA), and MycoZap™ Prophylactic (Cat No: VZA-2032, Lonza, Walkersville, MD). HUVEC cells were grown in VascuLife EnGS Endothelial Complete Medium (Cat No: LL-0002, Lifeline Technology, Frederick, MD). Lenti-Pac 293Ta cells (Cat No: CLv-PK-01) were purchased from Genecoepia (Rockville, MD) for lentiviral packaging. These cells were grown in DMEM-Glutamax media. All cells were grown at 37^0C in a 5% CO_2 incubator. Cell lines were regularly monitored for mycoplasma contamination using the mycoplasma MycoAlert detection kit (Cat No: LT07–318, Lonza, Walkersville, MD). All cell lines were periodically re-authenticated by STR profiling using one of two services (ATCC, Manassas, VA, or UAGC, Tucson, AZ). Unless otherwise indicated, cells were serum starved for 6–12 hours prior to treatments with either Ang II (1 μM), TNFa (10 ng/ml) or PBS vehicle, ± inhibitors as appropriate (IKK-VI, 1–5 μM; losartan, 5 μM).

Stable Transfections and Lentiviral Transductions

ZR75–1 cells were transfected with either pReceiver-AGTR1-FLAG (ZR751-AGTR1) or pReceiver-FLAG (ZR751-Neo) using Lipofectamine 2000 (ThermoFisher). After 48–72h, 0.4 mg/ml Geneticin (G418; Cat No: 10131027, ThermoFisher) was added to the media and cells were cultured for two weeks. Resulting G418-resistant clones were pooled and expanded further in the presence of 0.4 mg/ml G418.

Lentiviral plasmids harboring either control or Bcl10 shRNAs were transfected into 293Ta packaging cells using Lipofectamine 2000. Lentiviral particles were harvested, concentrated, and used to transduce ZR75-AGTR1 cells for 24 hours. Selection was accomplished by culturing in the presence of Puromycin and G418. Immunoblot analyses were used to verify either the maintenance or loss of Bcl10 in the resulting pools of stably transduced cells.

Transient siRNA Transfections

ON-TARGET plus SMARTpool siRNAs targeting CARMA3 (Cat No: L-004395–00-0020), Bcl10 (Cat No: L-004381–00-0020) and MALT1 (Cat No: L-005936–00-0020) were obtained from GE Dharmacon. Non-targeting siRNA pools (Cat No: D-001810–10-50) were used as controls. SMARTpool siRNAs (20 nM) were reverse transfected into BT549 or ZR75-AGTR1 cells using Lipofectamine RNAiMAX (ThermoFisher). Knockdown efficiencies were assessed using immunoblots and real-time quantitative RT-PCR assays (TaqMan) for the intended targets after 48–72 hours.

SDS-PAGE, Western Blotting, Quantitative RT-PCR, and Luciferase Assays

Cell lysates were prepared with RIPA buffer (Cat No: 89901, ThermoFisher) containing HALT Protease and Phosphatase Inhibitor cocktail (Cat No: 78440, ThermoFisher), loaded onto BioRad 4–15% gradient SDS-PAGE TGX gels, and transferred to 0.2μm nitrocellulose membranes (BioRad). Blots were then probed with the indicated primary antibodies (listed in Supplementary Methods) and developed using Pierce ECL Plus Western Blotting Substrate (Cat No: 32134). Total RNA was isolated from cell cultures and evaluated by RT-PCR using TaqMan gene expression assays (ThermoFisher) as described in Supplementary Methods. NF-κB reporter assays were performed as described previously (15) and as detailed in the Supplementary Methods.

Immunofluorescence and Confocal Microscopy

BT549 and ZR75 cells were plated on glass-bottom 35mm dishes (D35–20-0-N, Cellvis), 1 × 10^5 cells/dish. After treatment ± Ang II for 1 hour, cells were fixed with 2% paraformaldehyde and permeabilized with 0.1% Triton X-100 in PBS. Cells were then blocked for 60 minutes and incubated overnight with rabbit anti-RelA antibody (1:400), followed by goat anti-rabbit (Alexa Flour 488) secondary antibody (1:400) for 1 hour. Confocal microscopy was performed using a Zeiss LSM 710 with a 63X oil objective. Images were collected and processed using Zen software (Carl Zeiss, Inc.).

Cell Proliferation, Migration and Invasion Assays

2D cell proliferation was measured using the IncuCyte Live Cell Imaging system, according to the manufacturer's instructions (Essen BioScience). Spheroid growth was also measured in the IncuCyte and spheroid volume was quantified using SpheroidSizer, a MATLAB-based open-source application. Migration assays were performed following the IncuCyte ZOOM 96-well Scratch Wound Cell Migration assay protocol. Finally, invasion assays were performed using a modified Boyden chamber assay protocol. All methods are described in detail in Supplementary Methods.

Endothelial Chemotaxis

BT549 and ZR75-AGTR1 cells were transiently transfected with control or Bcl10 siRNA in 60 mm dishes (4 × 10^5 cells/dish). After 48 hours, cells were serum-starved overnight and treated ± Ang II for another 24 hours before collecting the resulting conditioned medium from the dishes. The collected medium was centrifuged at 1000 rpm for 10 min and filtered through a 0.2 μM membrane to remove intact cells or cellular debris. The conditioned medium was further concentrated using a Millipore Amicon ULTRA (3 kDa) filter (UFC800324, EMD Millipore), normalized and immediately used in the chemotaxis assay.

Neutralizing antibodies were added to some samples of conditioned medium as a cocktail of α-IL6 (250 ng/ml), α-IL8 (600ng/ml), α-IL1b (5ng/ml), α-VEGF-A (10 ng/ml), a-INHBA (100ng/ml), and α-SerpinE1 (400 ng/ml), and allowed to incubate for 30 minutes before proceeding to the chemotaxis assay. In parallel, isotype-matched IgG1 and IgG2b was added to control conditioned media at equivalent concentration.

Chemotaxis assays were performed using IncuCyte ClearView 96-well chemotaxis plates (Cat No: 4582, Essen BioScience) which contain transwell membranes punctuated with 96 laser-etched pores of 8 μM diameter. Briefly, both sides of the ClearView membranes were coated with Matrigel (50 μg/ml for 30 min at 37°C, followed by 30 min at room temp). Next, 2×10^3 HUVEC cells, re-suspended in 60 μl of 0.5% FBS VascuLife EnGS (LifeLine Cell Technology) endothelial cell medium (complete medium diluted 1:4 in EnGS basal medium), were added to the top chamber of ClearView 96-well inserts. Cells were allowed to adhere to the top surface of the ClearView membranes for 30 min at room temp. Concentrated conditioned medium (100 μl) from either BT549 or ZR75-AGTR1 cells was diluted 1:1 with 1% FBS-containing endothelial cell media (complete medium diluted 1:2 in EnGS basal medium) and the resulting 200 μl of diluted conditioned medium was added to each lower chamber. Images were obtained of both the top and bottom surfaces of each ClearView membrane every 2 hours for 4–6 days. The IncuCyte Chemotaxis Analysis software module was used to quantify migration of HUVEC cells towards the conditioned medium.

In Vivo Analyses in Mice and Chick embryos

All animal procedures were performed in accordance with the NIH and institutional guidelines, and were approved by the Institutional Animal Care and Use Committee (IACUC) at the University of Pittsburgh. The *in vivo* angiogenesis plug and traditional xenograft assays, as well as the CAM assay were performed as described in Supplementary Methods.

NanoString and Ingenuity Pathway Analysis (IPA)

RNA was extracted from BT549 cells 72 hours after siRNA transfection using the RNeasy Plus Kit (Qiagen) and quantified using NanoDrop, while quality was assessed using RNA Nano chips (Cat No: 5067–1511) on an Agilent 2100 Bioanalyzer. RNA Samples were then evaluated using the nCounter PanCancer Progression Panel (NanoString) according to the manufacturer's directions. Alternatively, samples were evaluated using a custom-designed probe panel consisting of 72 test genes and 6 housekeeping genes (see Supplementary Table 1). Briefly, 100 ng of total RNA was hybridized overnight at 65 °C, then run on a NanoString Prep Station at maximum sensitivity. Cartridges were scanned on a NanoString Digital Analyzer at 555 fields of view. Raw count data was normalized using the nSolver analysis software version 3.0, which normalizes samples according to positive and negative control probes and the geometric mean of six housekeeping probes. Genes with normalized counts less than 20 were considered as background and were not included in the analysis. IPA analyses of NanoString data were performed using the Core Analysis function of the IPA software, v.31823283 (Qiagen Bioinformatics).

Bioinformatics

Publicly available gene expression data were obtained from cited studies via CBioPortal (www.cbioportal.org), the UCSC Xena Browser (www.xena.ucsc.edu), and the NCBI Gene Expression Omnibus (www.ncbi.nlm.nih.gov/geo). Kernel density plots were generated using the CGDS-R and gtools packages in R (v3.0.2). Heat maps were generated using the Xena Browser and Morpheus (https://software.broadinstitute.org/morpheus). GSEA analyses

were performed using the GSEA software package (GSEA v2.2.3) and molecular signatures available from the Broad Institute. Clinical outcome analyses, including Kaplan-Meier analyses, were performed using GraphPad Prism (v7.01) and Minitab (v17.1.0) software packages.

Statistical Analysis

Statistical analyses were performed with GraphPad Prism software. *P* values were calculated using the Student *t* test (two sided) or by analysis of one-way ANOVA, followed by Bonferroni post-test as appropriate. Significance was determined at $p < 0.05$.

RESULTS

AGTR1 Overexpression Defines a Subset of Luminal Breast Cancers with Poor Prognosis

We previously demonstrated that AGTR1 overexpression characterizes a subset of HER2-negative breast cancers, based on MetaCOPA analysis of 31 independent microarray datasets published between 1999 and 2006 (5). Since that time, additional large datasets have become available, most notably the TCGA dataset which includes a complete analysis of >1000 breast cancers (16). To determine if the phenomenon of AGTR1 overexpression is recapitulated in the newer TCGA dataset, we evaluated RNA expression data using kernel density plot analysis. Results showed a striking bimodal distribution pattern for AGTR1 expression, with ~19.5% of cases falling within a group characterized by distinctly high levels of AGTR1 mRNA (Fig. 1A). Density plot analysis performed on the nearly 2000 invasive breast cancer cases profiled by METABRIC revealed a similar bimodal pattern, with 17.8% of cases showing aberrantly high AGTR1 (Supplementary Fig. S1A). Importantly, we found that AGTR1 and HER2 overexpression are mutually exclusive, with essentially no cases in the TCGA collection showing significantly high co-expression of the two receptors (Fig. 1B). When sorted by PAM50 subtype, AGTR1+ cases clustered within the ER+ (Luminal A and Luminal B) subgroups (Fig. 1C). Finally, we analyzed selected TCGA cases (originating from University of Pittsburgh) using RNA *in situ* hybridization (RNAscopeÒ) to confirm that high levels of AGTR1 mRNA revealed by the TCGA microarray analysis were in fact due to aberrant expression of the mRNA within malignant epithelial cells, as opposed to inflammatory cells or other stromal cells of the tumor microenvironment (Supplementary Fig. S1B).

If AGTR1 overexpression functionally drives pro-tumorigenic behavior, much like HER2, we might expect to find evidence that AGTR1+ breast cancers are among the more aggressive Luminal cancers. We therefore queried the TCGA collection of invasive ductal carcinomas to determine if AGTR1 levels correlate with TNM stage at diagnosis, and found a significant association between high AGTR1 expression and axillary node metastases (Fig. 1D). In addition, we applied gene set enrichment analysis (GSEA) to TCGA cases stratified by AGTR1 expression, using the van ‘t Veer 56 gene set (17), one of the first and most powerful multigene panels for prognostication. Strikingly, AGTR1+ tumors showed dramatic enrichment for genes linked to poor prognosis and development of distant metastasis within 5 years (Fig. 1E). We also queried the entirely separate Pusztai dataset which includes detailed clinical outcome data (18), and found that AGTR1 expression

inversely correlates with pathologic complete response (pCR) to neoadjuvant combination chemotherapy (Fig. 1F). Indeed, retrospective analysis of all 133 patients within the Pusztai dataset demonstrates that measurement of AGTR1 alone would have served as a statistically meaningful predictor of treatment resistance. Particularly notable is the fact that no patient with an AGTR1 level in the upper quartile experienced pCR (Fig. 1G). Finally, Kaplan-Meier curves generated from both the TCGA dataset and from the Gyorffy meta-analysis (19) demonstrate that AGTR1 overexpression correlates strongly with reduced breast cancer survival (Fig. 1H and I).

AGTR1 Overexpression Directs NF-κB-dependent Gene Expression Reprogramming in Breast Cancer Cells

Because HER2 and AGTR1 overexpression are mutually exclusive in breast cancer, we hypothesized that the most critical pathogenic signaling pathways for AGTR1 would likely be the pathways that are redundantly activated by HER2. While each receptor activates a range of intracellular signaling pathways relevant to cancer progression, both are capable of triggering the canonical NF-κB pathway and this represents an important node of potential signal convergence for these two receptors. NF-κB is a critically important transcription factor controlling expression of genes that drive breast cancer proliferation, survival, migration, invasion, and peritumoral angiogenesis (20, 21). Thus, we looked for evidence that AGTR1 overexpression drives an NF-κB gene expression signature in breast cancer by specifically querying NF-κB gene targets that are known to be expressed in epithelial cells and that have been highlighted in the breast cancer literature. Strikingly, many of the genes that meet these criteria are substantially upregulated in AGTR1+ invasive breast cancers from the TCGA collection (Fig. 2A). These include genes that affect pathogenic processes such as survival and proliferation (eg, *BCL2, CCND1, DUSP6, TNFRSF10C*), migration and invasion (eg, *IL1β , PCSK6, CSF1, JAG1, ZEB1, SAA1*), stemness (eg, *CD44, BMPR1B, DCLK1, JAG1*), and angiogenesis (eg, *IL1β, NPY1R, IL6ST/GP130*) among others.

Given the association between AGTR1 overexpression and upregulation of key pathogenic NF-κB target genes in clinical samples, we sought to directly test if AGTR1 drives NF-κB activity in established cell model systems. Although we had previously identified several breast cancer cell lines with high endogenous AGTR1 expression (5), we revisited the analysis using the newer expression profiling data available through the Cancer Cell Line Encyclopedia (CCLE) (22). Results showed that the BT549 cell line ranks near the top of all breast cancer lines when stratified for AGTR1 expression; in contrast, ZR75–1 cells have essentially undetectable levels of AGTR1 mRNA (Supplementary Fig. S1C). Established cell lines with significant AGTR1 overexpression are uniformly HER2-negative, but interestingly many also lack ER, unlike what we find in clinical samples of primary breast tumors, where AGTR1 tends to be co-expressed with ER. The reason for this difference is unclear but may relate to alterations in ER expression that can occur with prolonged culture *in vitro*. In contrast, the ZR75–1 cell line belongs to the ER+/HER2- Luminal subcategory (23), and therefore the same subcategory of breast cancer in which AGTR1 overexpression can be seen clinically. To simulate acquired AGTR1 overexpression in this subcategory, we created derivative ZR75–1 lines by stably transfecting the parental line with an AGTR1

expression vector (ZR75-AGTR1), or an empty vector as a negative control (ZR75-neo) (Supplementary Fig. S1D). Finally, we experimentally confirmed AGTR1, ER, PR and HER2 status in all lines by quantitative RT-PCR (Supplementary Fig. S1E and F). Together, the BT549 and ZR75-AGTR1 lines provide complementary models of high-level endogenous and exogenous AGTR1 expression, respectively. For secondary analyses and to confirm observations made with these principal models, we selected the Hs578T and Hs606T cell lines which, like BT549 cells, are among the breast cancer lines with the highest endogenous AGTR1 expression (Supplementary Fig. S1C).

In ZR75–1 cells, we found that overexpression of AGTR1 alone confers significant NF-κB activation, as evidenced by moderate, constitutive RelA (p65) nuclear translocation in ZR75-AGTR1 cells relative to control ZR75-neo cells (Fig. 2B and C). Compared to ZR75-neo cells, BT549 cells, which express high levels of endogenous AGTR1, also show enhanced nuclear RelA at baseline (Supplementary Fig. S2A). In ZR75-AGTR1 cells, this increase in basal nuclear RelA is reflected by a >20-fold increase in NF-κB-dependent transcriptional activity at baseline, as measured by expression of a transfected NF-κB-luciferase reporter (Fig. 2D). Despite the elevated basal NF-κB activity, treatment of ZR75-AGTR1 cells with Angiotensin II ligand (Ang II) results in even greater NF-κB activation (~4-fold more than ZR75-AGTR1 cells under basal conditions and >100-fold more than the level observed in ZR75-neo cells) (Fig. 2B-D). BT549 cells similarly respond to Ang II with an increase in NF-κB nuclear translocation and NF-κB-luciferase reporter activity (Supplementary Fig. S2A and B). For both ZR75-AGTR1 and BT549 cells, we confirmed that this ligand-dependent NF-κB activation proceeds through AGTR1 and the canonical NF-κB pathway by demonstrating that it is completely blocked via pre-treatment with either losartan (an AGTR1-specific antagonist), or IKK-VI (an IKKβ-specific inhibitor) (Supplementary Fig. S2B).

The acute, ligand-induced burst of NF-κB signaling is best demonstrated by Western blot analysis of p-IkB. Accordingly, we found that while ZR75-neo cells show no detectable increase in p-IkB following Ang II stimulation, both ZR75-AGTR1 and BT549 cells respond to Ang II with an acute increase in p-IkB that is similar in magnitude to that achieved by stimulating cells with TNFa (Fig. 2E). Hs578T and Hs606T cells, which like BT549 cells also express high endogenous AGTR1, respond to Ang II with similar time-dependent generation of p-IkB (Supplementary Fig. S3A). Importantly, the magnitude of Ang II-dependent p-IkB induction in BT549 cells is comparable to that seen constitutively in SKBR3 cells, which overexpress HER2 (Fig. 2F).

To rule out the possibility that the basal NF-κB activity in cells expressing high AGTR1 levels might be due to an autocrine loop, with cells producing and secreting Ang II ligand, we performed ELISAs on media collected from both ZR75-AGTR1 and BT549 cells. Ang II was undetectable in media taken from these cells following 1–3 days in culture, while Ang II was clearly detected in media taken from the culture of CRL-7548 placental cells which are known to produce and secrete low levels of Ang II (24) (Fig. 2G). These results are in keeping with previous work indicating that many GPCRs, including AGTR1, exhibit measurable basal signaling activity that is enhanced further by ligand stimulation (25–27). Thus, overexpression of AGTR1 confers both significant, ligand-independent (basal) NF-κB

activity while sensitizing cells to further bursts of NF-κB activity initiated by exposure to the Ang II ligand. These bursts of NF-κB activity are capable of reaching levels seen in HER2+ breast cancer cells.

The CARMA3/Bcl10/MALT1 Signalosome Mediates NF-κB Activation in AGTR1+ Breast Cancer Cells

Our laboratory previously described a signaling pathway in vascular endothelial cells that mediates NF-κB activation downstream of AGTR1 (28, 29). This signaling pathway is analogous to the well-known pathway that is operative in immune cells downstream of antigen receptors, and relies on PKC-dependent assembly of a signaling module comprised principally of the triad of CARMA3 (a scaffolding protein), Bcl10 (a small linker protein), and MALT1 (an effector protein), also known as the CBM signalosome (10, 11, 30, 31). In endothelial cells, AGTR1 triggers the CBM signalosome to direct NF-κB-dependent pro-inflammatory responses that contribute to endothelial dysfunction and vascular disease (15, 29, 32, 33).

We therefore asked if the same CBM signalosome drives NF-κB activation in breast cancers harboring AGTR1 overexpression. To this end, we used siRNA to individually target each component of the CBM signalosome in both BT549 and ZR75-AGTR1 cells, and tested the impact on Ang II-dependent p-IkB induction. Results demonstrated that in both cell models, knockdown of either CARMA3, Bcl10, or MALT1 completely abrogates the p-IkB response (Fig. 3A). Hs578T and Hs606T cells show a similar complete dependence on the CBM signalosome for Ang II-dependent p-IkB induction (Supplementary Fig. S3B). Notably, the inhibitory effect of knocking down the CBM components is comparable to the effect of treating cells with either losartan or the IKKb inhibitor, IKK-VI (Fig. 3B). These results suggest that the AGTR1-CBM-NF-κB signaling axis has impact that extends beyond its role in vascular inflammation, and into the arena of solid tumor pathogenesis.

The CARMA3/Bcl10/MALT1 Signalosome Critically Influences Gene Expression Reprogramming in AGTR1+ Breast Cancer Cells

We next tested the impact of disabling the CBM signalosome on NF-κB –dependent gene expression reprograming by targeting Bcl10, the central adaptor protein within the complex. Using siRNA, we knocked down Bcl10 in BT549 cells and assessed alterations in gene expression using a custom NanoString codeset designed to simultaneously measure 72 NF-κB regulated mRNAs, the products of which all have known roles in cancer progression (Supplementary Table 1). We designed the custom codeset to measure selected genes that we had previously found to be induced in AGTR1+ human breast cancer specimens (see Fig. 2A), as well as additional potential NF-κB targets. Of the 72 genes, we found that 41 can be reliably quantified in BT549 cells by the NanoString assay and cluster within several discrete groups. First, a substantial number are strongly induced by Ang II in BT549 cells, particularly after 24 hours of stimulation, but are not induced in cells with siRNA-mediated Bcl10 knockdown (Group A) (Fig. 3C). A second group is composed of genes that required Bcl10 for both basal and Ang II-induced expression (Group B). These results are consistent with our observation that AGTR1 over-expression mediates both basal and Ang II-responsive NF-κB activity in breast cancer cells. Thus, genes in Group B appear to be

particularly sensitive targets, and are induced by basal AGTR1/CBM/NF-κB signaling activity, while those in Group A require ligand-activated AGTR1/CBM/NF-κB signaling to be significantly induced. Finally, smaller subsets of genes are induced by Bcl10 knockdown (Group C) or are not substantially impacted (Group D) (Fig. 3C).

We then tested the impact of Bcl10 knockdown on the broader gene expression landscape, by using the NanoString PanCancer Progression codeset, which quantifies expression of 770 genes of significance to solid tumor pathogenesis, most of which are not necessarily NF-κB target genes. Knockdown of Bcl10 in BT549 cells caused a dramatic shift in the gene expression program, with many genes being either up- or down-regulated (Fig. 3D). This result suggests that disruption of the Bcl10/NF-κB signaling pathway has far-reaching effects that ultimately impact multiple gene networks through complex and potentially indirect mechanisms. To better understand the overall pathophysiologic impact of Bcl10 knockdown, we performed Ingenuity Pathway Analysis (IPA) with the NanoString data and found evidence for disruption of at least three cancer hallmark processes: (1) proliferation and survival, (2) invasion and metastasis, and (3) tumor angiogenesis (Fig. 3E). Specifically, Bcl10 knockdown leads to upregulation of tumor suppressor pathways (PTEN and p53), as well as enhanced apoptosis signaling (Fig. 3E, *left*). Conversely, Bcl10 knockdown leads to decreased activity in growth factor and motility signaling networks (Fig. 3E, *middle*). Finally, Bcl10 knockdown suppresses key angiogenesis pathways, including those for IL-6, IL-8, and VEGF (Fig. 3E, *right*).

The CARMA3/Bcl10/MALT1 Signalosome Controls Pro-tumorigenic Phenotypes in AGTR1+Breast Cancer Cells

Given the broad impact of Bcl10 knockdown on the pro-tumorigenic gene expression signature in AGTR1+ breast cancer cells, we sought to experimentally determine which pro-tumorigenic phenotypes, highlighted by the pathway analysis, are most clearly dependent on the CBM/NF-κB pathway. In addition, because we had observed that Bcl10 knockdown impacts both basal and Ang II-dependent gene expression, we wanted to determine which CBM/NF-κB-driven phenotypes are evident in the basal state, and which require Ang II stimulation.

We first tested the impact of pharmacologic NF-κB inhibition on the cell-intrinsic properties of proliferation, migration, and invasion in the basal state (without Ang II stimulation). In this setting, proliferation was the phenotype most significantly impacted by NF-κB inhibition; results showed that treatment of either ZR75-AGTR1 or BT549 cells with IKK-VI, an IKKb inhibitor, dramatically impairs cell proliferation as monitored in 2D cultures (Fig. 4A and B). Next, we tested the effect of CBM disruption and found that proliferation is likewise impaired upon siRNA-mediated CARMA3 or MALT1 knockdown (Fig. 4C and D). We explored this phenomenon further using 3D spheroid assays, and found that IKK-VI also exerts a dramatic inhibitory effect on spheroid growth (Fig. 4E and F). Disruption of the CBM complex, via knockdown of any of the three components, in either ZR75-AGTR1 or BT549 cells similarly inhibits spheroid growth (Fig. 4G and H; Supplementary Fig. S4A and S4B). Finally, we evaluated the additional AGTR1+ cell lines, Hs578T and Hs606T, and found that basal proliferation in these cells is again abrogated by knockdown of the CBM

components (Supplementary Fig. S4C and S4D). Since these 2D and 3D proliferation assays were performed in the absence of exogenous Ang II, the results suggest that signaling through the CBM/NF-κB pathway occurs under basal conditions in AGTR1+ breast cancer cells, to impart a positive proliferative advantage.

Because stimulating AGTR1+ breast cancer cells with exogenous Ang II induces NF-κB levels beyond those seen in the basal state (see Fig. 2), we asked if additional pro-tumorigenic phenotypes are revealed under this ligand-stimulated condition, to complement the increase in proliferation that occurs in the absence of added ligand. We found that Ang II stimulation significantly increases migration of both ZR75-AGTR1 and BT549 cells in a kinetic wound-healing assay and that this is completely abrogated by Bcl10 knockdown (Fig. 5A-D). Further, Ang II stimulation promotes invasion of both cell lines through matrigel, as assessed in a transwell invasion assay, and this is similarly blocked by Bcl10 knockdown (Fig. 5E-H). These findings are recapitulated in Hs578T and Hs606T cells; both of these AGTR1+ lines respond to Ang II with an increase in migration and invasion that is abrogated upon Bcl10 knockdown (Supplementary Fig. S5A-S5D). Taken together, these results indicate that AGTR1 overexpression confers both a constitutive proliferative advantage to breast cancer cells as well as a ligand-responsive migration and invasion advantage, all of which critically depend on signaling through the CBM/NF-κB axis.

The CARMA3/Bcl10/MALT1 Signalosome Controls Paracrine Signaling to Endothelial Cells, Driving Endothelial Chemotaxis

Because our gene expression data strongly implicated the CBM pathway in regulating an angiogenic gene signature, we asked if AGTR1+ cells exert a pro-angiogenic effect through paracrine stimulation of neighboring endothelial cells. To this end, we established a real-time, kinetic assay for monitoring endothelial chemotaxis. In this assay, we utilized specialized IncuCyte™ transwells that consist of upper and lower chambers separated by an impermeable surface punctuated by regularly spaced, 8 μM channels that are large enough to allow for endothelial cell transmigration (Fig. 6A). We plated primary human umbilical vein endothelial cells (HUVECs) in the upper chamber, along with regular media, and used the real-time imaging capabilities of the IncuCyte™ system to measure movement of HUVECs through the channels to the lower chamber when filled with conditioned media obtained from AGTR1+ breast cancer cells. Because the system can simultaneously image cells in the top and bottom chambers, applying a pseudo-color (blue and yellow, respectively) to distinguish the two populations, it is possible to quantify endothelial cell migration over time.

In control experiments, we found that media that has never been exposed to breast cancer cells has minimal impact on the migration of endothelial cells to the bottom chamber, regardless of whether or not this control media contains exogenously added Ang II (Fig. 6B and D, top row of images; quantified in Fig. 6C and E). In contrast, conditioned media obtained from the culture of either ZR75-AGTR1 or BT549 cells, transfected with non-targeting siRNA, strongly enhances endothelial chemotaxis, but only when the breast cancer cells have been stimulated by Ang II (Fig. 6B-E). Conditioned media from breast cancer cells with siRNA-mediated knockdown of Bcl10, however, is unable to induce endothelial

chemotaxis above baseline (Fig. 6B-E). These data suggest that Ang II stimulation of AGTR1+ breast cancer cells results in secretion of one or more substances that support endothelial chemotaxis, and that this is a Bcl10-dependent process.

Based on our gene expression profiling results employing Bcl10 knockdown (Fig. 3C and D), there are numerous candidate molecules that could fulfill the role of an endothelial chemotactic factor (Supplementary Table 2). To begin deconvoluting this list with the goal of identifying the most important factor(s), we prepared a mix of neutralizing antibodies against six particularly promising candidates, IL-1β, IL-6, IL-8, SERPINE1 (PAI-1), VEGFA, and INHBA. We then added the neutralizing antibody cocktail, or isotype-matched control IgG cocktail, to conditioned media from Ang II-treated BT549 cells, and then utilized the media in the chemotaxis assay. Remarkably, we found that the neutralizing antibody cocktail specifically and completely inhibits the induced endothelial chemotaxis (Fig. 6F). Further work will be required to determine which of these six factors might be most important for the Bcl10-dependent endothelial chemotaxis phenomenon, or if a specific combination of factors is critical.

Bcl10 is Required for AGTR1+ Tumor Angiogenesis *in vivo*

Finally, we tested if the Ang II/Bcl10-dependent endothelial chemotaxis observed *in vitro* correlates with cancer cell-induced angiogenesis in an *in vivo* model. To this end, we mixed Ang II-treated breast cancers cells with concentrated, growth-factor depleted Cultrex to create a semi-solid suspension that can be implanted subcutaneously in athymic nude mice. These implanted “plugs”, containing breast cancer cells, then serve as a matrix for the potential ingrowth of host vasculature over the next 12–14 days, dependent on angiogenic signals provided by the embedded cancer cells. Compared to plugs of control ZR75-neo cells, we found that ZR75-AGTR1 plugs show grossly obvious, enhanced vascularization (Fig. 7A). We confirmed this observation by quantifying plug hemoglobin content, a measurement of functional vascular content (Fig. 7B). Plugs formed with ZR75-AGTR1 cells engineered to stably express a non-targeting shRNA are similar to those composed of parental ZR75-AGTR1 cells. In contrast, plugs formed from ZR75-AGTR1 cells expressing Bcl10 shRNA are visibly pale and grossly lacking in vascularization, more similar to ZR75-neo plugs, a finding confirmed by measurement of hemoglobin content (Fig. 7C and D). Of importance, all plugs were prepared using cells treated with Ang II at the time of subcutaneous implantation, since we had found that AGTR1+ cancer cells must be stimulated with Ang II in order to drive endothelial chemotaxis *in vitro*.

Taken together, the *in vitro* and *in vivo* results suggest that AGTR1+ breast cancers are capable of supporting tumor angiogenesis through the CBM/NF-κB signaling axis. This cell-extrinsic effect likely synergizes with the cell-intrinsic effects of the CBM pathway in supporting tumor cell proliferation, migration, and invasion.

Bcl10 is Required for Overall AGTR1+ Breast Cancer Growth and Host Tissue Disruption *in vivo*

Results presented above indicate that the CBM/NF-κB signaling axis controls a range of specific phenotypes in the context of AGTR1+ breast cancer. These include cancer cell

proliferation, migration and invasion, as well as induced angiogenesis. To determine if the CBM complex controls overall tumorigenesis as an integrated outcome of these specific phenotypes, we performed traditional xenograft growth experiments. We found that xenografts consisting of ZR75 cells with enforced expression of AGTR1 (ZR75-AGTR1) grow significantly faster than those consisting of control ZR75 cells, ultimately producing larger, heavier tumors (Fig. 7E-G). Knockdown of Bcl10 via stable shRNA expression dramatically reverses tumor growth, while control shRNA expression has no effect (Fig. 7E-G). In keeping with results from the angiogenesis plug assay, ZR75-AGTR1 xenografts show gross evidence of enhanced vascularization, as compared to ZR75-neo xenografts (Fig. 7E). Moreover, knockdown of Bcl10 appears to prevent efficient vascularization of mature xenografts, in addition to abrogating tumor growth.

To evaluate tissue invasion, we turned to the chick chorioallantoic membrane (CAM) model. Here, we layered Ang II-treated ZR75-AGTR1 cells, with or without Bcl10 knockdown, on the surface of the living chick membranes and observed the resulting interaction between cancer cells and the host tissue after a short, four-day period. Results showed that ZR75-AGTR1 cells expressing control shRNA induce a remarkably robust host tissue response characterized by acute neutrophilic inflammation, edema, fibroblast proliferation, reactive epithelial metaplasia of the surface epithelium, and overall superficial connective tissue disruption (Fig. 7H). These features result in an irregular tumor cell/host tissue interface that resembles the invasive, leading front of an aggressive infiltrating carcinoma. In contrast, ZR75-AGTR1 cells expressing Bcl10 shRNA remain completely quiescent on the surface of the CAM and show almost no discernable effect on the underlying host membrane (Fig. 7H). Taken together, these two *in vivo* models suggest that the CBM signalosome plays a central role in the overall growth and vascularization of AGTR1+ breast cancers and in instigating local, tissue-destructive, inflammatory responses in the surrounding host parenchyma that may facilitate invasion.

DISCUSSION

NF-κB activation is well-described in aggressive breast cancer, particularly for the HER2+ intrinsic subtype (20, 21, 34). Yet the regulation of NF-κB and its potential pathogenic role in luminal breast cancer is not well characterized. Our group previously identified a subset of luminal breast cancers that harbor dramatic overexpression of AGTR1, a GPCR best known for its role in the vasculature (5). With the current work, we now provide a mechanistic understanding of how AGTR1 overexpression recapitulates aggressive features of HER2+ cancer by harnessing a signaling complex composed of the proteins CARMA3, Bcl10, and MALT1 (CBM signalosome) to affect NF-κB activation.

Importantly, we demonstrate that the CBM pathway exerts not only cell-intrinsic effects on tumor cell proliferation, migration, and invasion, but also cell-extrinsic effects by impacting non-neoplastic cells of the tumor microenvironment. Specifically, we show that conditioned media from Ang II-stimulated, AGTR1+ breast cancer cells induces endothelial cell chemotaxis *in vitro* and promotes tumor angiogenesis *in vivo*. Numerous CBM/NF-κB responsive target genes are likely to mediate the cell-intrinsic and cell-extrinsic effects, with different subsets of genes controlling each (see schematic, Fig. 7I). Based on our *in silico*

and experimental analyses, there are a large number of secreted substances that could be released from AGTR1+ tumor cells in a CBM/NF-κB dependent manner and act in paracrine fashion on neighboring endothelial cells (Fig. 7I). These include IL-1β, IL-8, IL-6, INHBA, SERPINE1, and VEGF, all of which have prominent roles in regulating tumor angiogenesis, along with many other candidates (35, 36). We are now working to systematically deconvolute the secretome of AGTR1+ breast cancer cells, which should provide further insights into this paracrine effect. In addition, it will be important to determine if any of these secreted substances influence other cells of the tumor microenvironment, such as adipocytes, fibroblasts, or cells of the immune system including neutrophils, T cells, macrophages, and myeloid derived suppressor cells (MDSCs), particularly in light of the fact that our CAM assays demonstrate that ZR75-AGTR1 cells induce a markedly robust host inflammatory response. IL-1β represents an intriguing candidate effector in this regard, since it has well-recognized roles in modulating the immune contexture of breast cancer to promote immunologic tolerance and support both local and metastatic growth (37–39). IL-1β may also affect resident stromal cells of the breast; a recent report demonstrated that IL-1β production in breast cancer stimulates adipocyte-derived VEGF that in turn drives angiogenesis (40). Thus, CBM/NF-κB dependent IL-1β production could initiate a cascade of events affecting multiple, interacting cells of the tumor microenvironment.

While our study demonstrates a pathogenic role for CBM-dependent NF-κB activation downstream of AGTR1 in a specific subset of breast cancers, we speculate that the CBM signalosome may act as a central signaling node for other subsets of breast cancer characterized by overexpression or hyperactivity of related GPCRs. Several GPCRs implicated as oncogenic drivers in breast cancer, including protease-activated receptor 1 (PAR1), C-X-C chemokine receptor 4 (CXCR4), and the lysophosphatidic acid receptors (LPAR1 and LPAR3) each require the CBM signalosome to elicit NF-κB activation in a variety of contexts (11, 31). The common mechanism appears to be that each receptor activates specific PKC isoforms that phosphorylate CARMA3, allowing for CBM complex assembly. Thus, it will be important to address whether ligand-dependent activation of these related GPCRs can drive the aggressive phenotypes of proliferation, invasion, and migration in a manner that similarly requires CBM signaling. Finally, Xin Lin and collaborators recently reported the surprising finding that specific tyrosine kinase receptors can also harness the CBM signalosome (41, 42). Using both lung and breast models, these authors demonstrated that both heregulin and EGF induce NF-κB via a PKC-CBM pathway. In both cases, CBM signaling was required for *in vitro* cell proliferation, migration, and invasion. Further, the authors found that genetic MALT1 deficiency blocked *in vivo* tumorigenesis in two elegant models of HER2- and EGFR-driven breast and lung cancer. Taken together, our studies and those of the Lin group suggest that the CBM complex represents a central signaling node upon which multiple receptor-mediated signals may converge to drive pathogenic NF-κB activation in solid tumors.

We speculate that therapeutically targeting MALT1 may be a rational and effective approach for treating a range of breast cancers, given the prominent role of the CBM signaling pathway in AGTR1+ breast cancer and possibly in those driven by related GPCRs, or even HER family members. Recently, several potent small molecule inhibitors of MALT1 have

been characterized that block the protease function of MALT1, necessary for its full induction of NF-κB target genes (43, 44). These inhibitors include members of the phenothiazine class (mepazine, thioridazine, promazine) as well as a novel compound, MI-2. Importantly, these MALT1 inhibitors are effective at blocking growth of Diffuse Large B Cell Lymphomas (DLBCLs) that are driven by activating mutations in CARMA1 (the lymphocyte homologue of CARMA3), thereby providing proof-of-concept for their effectiveness in malignancies characterized by unmitigated CBM/NF-κB activity (43–45). By analogy, we suspect that these MALT1 inhibitors may also show efficacy against solid tumors such as the AGTR1+ subset of breast cancer. Interestingly, multiple groups have shown that mice harboring homozygous knock-in of a protease dead MALT1 allele, thereby mimicking complete and sustained pharmaceutical MALT1 inhibition, eventually develop a striking auto-immune phenotype (13, 46). This phenotype is due to the development of an imbalance in T cells, wherein loss of MALT1 protease activity preferentially reduces differentiation of Treg cells while leaving Th1 and Th2 effector cells relatively intact and functional (13, 46). This result suggests that use of a MALT1 inhibitor in the setting of a solid tumor, such as AGTR1+ breast cancer, might have dual efficacy in that it could (a) abrogate CBM-dependent, pro-tumorigenic activity within tumor cells and (b) simultaneously alter the immune contexture to favor anti-tumor immunity. In this context, MALT1 inhibition would theoretically leverage the dual role of MALT1 in both cancer cells and lymphocytes to synergistic benefit.

In summary, the work described herein characterizes a novel subtype of breast cancer, defined by AGTR1 overexpression in the absence of HER2 expression. These tumors, while largely confined to the luminal A and B categories, show surprisingly aggressive behavior and poor outcome. Our mechanistic studies demonstrate that the CBM signalosome drives a range of pathogenic phenotypes in the AGTR1+ subtype and nominate MALT1 as a potential therapeutic target. Given that the phenothiazine class of MALT1 inhibitors have been used clinically for other indications, the opportunity exists for their relatively rapid redeployment in the setting of AGTR1+ breast cancer. Finally, since the CBM signalosome may also function downstream of related GPCRs, or even HER2, in other subtypes of breast cancer, MALT1 inhibitors could have even broader therapeutic potential.

Supplementary Material

Refer to Web version on PubMed Central for supplementary material.

Acknowledgements

The authors thank Kimberly Fuhrer for her work in optimizing the RNA ISH analysis of AGTR1 expression and Anthony Green for expert assistance with histopathology.

Grant support: This work was supported in part by funding from the NIH (R01 HL082914 to P.C. Lucas and L.M. McAllister-Lucas) and by a grant from the Cancer Research Fund of the University of Michigan Comprehensive Cancer Center (to P.C. Lucas). J-Y Lee was supported by a RAC Fellowship Award from the Children's Hospital of Pittsburgh of UPMC. Dong Hu was supported by a gift from the NSABP Foundation. This project also used the University of Pittsburgh Cancer Institute (UPCI) Tissue and Research Pathology Services (TARPS) core facilities that are supported in part by award P30 CA047904.

REFERENCES

1. Senkus E, Cardoso F, Pagani O. Time for more optimism in metastatic breast cancer? Cancer Treat Rev 2014;40:220–8. [PubMed: 24126121]
2. Arteaga CL, Engelman JA. ERBB receptors: from oncogene discovery to basic science to mechanism-based cancer therapeutics. Cancer Cell 2014;25:282–303. [PubMed: 24651011]
3. Bianchini G, Balko JM, Mayer IA, Sanders ME, Gianni L. Triple-negative breast cancer: challenges and opportunities of a heterogeneous disease. Nat Rev Clin Oncol 2016;13:674–90. [PubMed: 27184417]
4. Tran B, Bedard PL. Luminal-B breast cancer and novel therapeutic targets. Breast Cancer Res 2011;13:221. [PubMed: 22217398]
5. Rhodes DR, Ateeq B, Cao Q, Tomlins SA, Mehra R, Laxman B, et al. AGTR1 overexpression defines a subset of breast cancer and confers sensitivity to losartan, an AGTR1 antagonist. Proc Natl Acad Sci U S A 2009;106:10284–9. [PubMed: 19487683]
6. Mehta PK, Griendling KK. Angiotensin II cell signaling: physiological and pathological effects in the cardiovascular system. Am J Physiol Cell Physiol 2007;292:C82–97. [PubMed: 16870827]
7. Dorsam RT, Gutkind JS. G-protein-coupled receptors and cancer. Nat Rev Cancer 2007;7:79–94. [PubMed: 17251915]
8. Hunyady L, Catt KJ. Pleiotropic AT1 receptor signaling pathways mediating physiological and pathogenic actions of angiotensin II. Mol Endocrinol 2006;20:953–70. [PubMed: 16141358]
9. Oh E, Kim JY, Cho Y, An H, Lee N, Jo H, et al. Overexpression of angiotensin II type 1 receptor in breast cancer cells induces epithelial-mesenchymal transition and promotes tumor growth and angiogenesis. Biochim Biophys Acta 2016;1863:1071–81. [PubMed: 26975580]
10. Juilland M, Thome M. Role of the CARMA1/BCL10/MALT1 complex in lymphoid malignancies. Curr Opin Hematol 2016;23:402–9. [PubMed: 27135977]
11. Rosebeck S, Rehman AO, Lucas PC, McAllister-Lucas LM. From MALT lymphoma to the CBM signalosome: three decades of discovery. Cell Cycle 2011;10:2485–96. [PubMed: 21750409]
12. Lang CC, Struthers AD. Targeting the renin-angiotensin-aldosterone system in heart failure. Nat Rev Cardiol 2013;10:125–34. [PubMed: 23319100]
13. Demeyer A, Staal J, Beyaert R. Targeting MALT1 Proteolytic Activity in Immunity, Inflammation and Disease: Good or Bad? Trends Mol Med 2016;22:135–50. [PubMed: 26787500]
14. Jaworski M, Thome M. The paracaspase MALT1: biological function and potential for therapeutic inhibition. Cell Mol Life Sci 2016;73:459–73. [PubMed: 26507244]
15. Delekta PC, Apel IJ, Gu S, Siu K, Hattori Y, McAllister-Lucas LM, et al. Thrombin-dependent NF-{kappa}B activation and monocyte/endothelial adhesion are mediated by the CARMA3.Bcl10.MALT1 signalosome. J Biol Chem 2010;285:41432–42. [PubMed: 21041303]
16. Cancer Genome Atlas N. Comprehensive molecular portraits of human breast tumours. Nature 2012;490:61–70. [PubMed: 23000897]
17. van ‘t Veer LJ, Dai H, van de Vijver MJ, He YD, Hart AA, Mao M, et al. Gene expression profiling predicts clinical outcome of breast cancer. Nature 2002;415:530–6. [PubMed: 11823860]
18. Hess KR, Anderson K, Symmans WF, Valero V, Ibrahim N, Mejia JA, et al. Pharmacogenomic predictor of sensitivity to preoperative chemotherapy with paclitaxel and fluorouracil, doxorubicin, and cyclophosphamide in breast cancer. J Clin Oncol 2006;24:4236–44. [PubMed: 16896004]
19. Gyorffy B, Surowiak P, Budczies J, Lanczky A. Online survival analysis software to assess the prognostic value of biomarkers using transcriptomic data in non-small-cell lung cancer. PLoS One 2013;8:e82241. [PubMed: 24367507]
20. Aggarwal BB. Nuclear factor-kappaB: the enemy within. Cancer Cell 2004;6:203–8. [PubMed: 15380510]
21. Shostak K, Chariot A. NF-kappaB, stem cells and breast cancer: the links get stronger. Breast Cancer Res 2011;13:214. [PubMed: 21867572]
22. Barretina J, Caponigro G, Stransky N, Venkatesan K, Margolin AA, Kim S, et al. The Cancer Cell Line Encyclopedia enables predictive modelling of anticancer drug sensitivity. Nature 2012;483:603–7. [PubMed: 22460905]

23. Jonsson G, Staaf J, Olsson E, Heidenblad M, Vallon-Christersson J, Osoegawa K, et al. High-resolution genomic profiles of breast cancer cell lines assessed by tiling BAC array comparative genomic hybridization. Genes Chromosomes Cancer 2007;46:543–58. [PubMed: 17334996]
24. Pan N, Frome WL, Dart RA, Tewksbury D, Luo J. Expression of the renin-angiotensin system in a human placental cell line. Clin Med Res 2013;11:1–6. [PubMed: 22997355]
25. Miura S, Saku K. The possible constitutive activity of wild-type angiotensin II type 1 receptor. Hypertens Res 2014;37:614–5. [PubMed: 24621462]
26. Tao YX. Constitutive activation of G protein-coupled receptors and diseases: insights into mechanisms of activation and therapeutics. Pharmacol Ther 2008;120:129–48. [PubMed: 18768149]
27. Unal H, Karnik SS. Constitutive activity in the angiotensin II type 1 receptor: discovery and applications. Adv Pharmacol 2014;70:155–74. [PubMed: 24931196]
28. McAllister-Lucas LM, Ruland J, Siu K, Jin X, Gu S, Kim DS, et al. CARMA3/Bcl10/MALT1-dependent NF-kappaB activation mediates angiotensin II-responsive inflammatory signaling in nonimmune cells. Proc Natl Acad Sci U S A 2007;104:139–44. [PubMed: 17101977]
29. McAllister-Lucas LM, Jin X, Gu S, Siu K, McDonnell S, Ruland J, et al. The CARMA3-Bcl10-MALT1 signalosome promotes angiotensin II-dependent vascular inflammation and atherogenesis. J Biol Chem 2010;285:25880–4. [PubMed: 20605784]
30. Meininger I, Krappmann D. Lymphocyte signaling and activation by the CARMA1-BCL10-MALT1 signalosome. Biol Chem 2016;397:1315–33. [PubMed: 27420898]
31. Wegener E, Krappmann D. CARD-Bcl10-Malt1 signalosomes: missing link to NF-kappaB. Sci STKE 2007;2007:pe21.
32. Marko L, Henke N, Park JK, Spallek B, Qadri F, Balogh A, et al. Bcl10 mediates angiotensin II-induced cardiac damage and electrical remodeling. Hypertension 2014;64:1032–9. [PubMed: 25185127]
33. Klei LR, Hu D, Panek R, Alfano DN, Bridwell RE, Bailey KM, et al. MALT1 Protease Activation Triggers Acute Disruption of Endothelial Barrier Integrity via CYLD Cleavage. Cell Rep 2016;17:221–32. [PubMed: 27681433]
34. Biswas DK, Iglehart JD. Linkage between EGFR family receptors and nuclear factor kappaB (NF-kappaB) signaling in breast cancer. J Cell Physiol 2006;209:645–52. [PubMed: 17001676]
35. Carmeliet P, Jain RK. Molecular mechanisms and clinical applications of angiogenesis. Nature 2011;473:298–307. [PubMed: 21593862]
36. Ono M Molecular links between tumor angiogenesis and inflammation: inflammatory stimuli of macrophages and cancer cells as targets for therapeutic strategy. Cancer Sci 2008;99:1501–6. [PubMed: 18754859]
37. Zitvogel L, Kepp O, Galluzzi L, Kroemer G. Inflammasomes in carcinogenesis and anticancer immune responses. Nat Immunol 2012;13:343–51. [PubMed: 22430787]
38. Voronov E, Dotan S, Krelin Y, Song X, Elkabets M, Carmi Y, et al. Unique Versus Redundant Functions of IL-1alpha and IL-1beta in the Tumor Microenvironment. Front Immunol 2013;4:177. [PubMed: 23847618]
39. Apte RN, Dotan S, Elkabets M, White MR, Reich E, Carmi Y, et al. The involvement of IL-1 in tumorigenesis, tumor invasiveness, metastasis and tumor-host interactions. Cancer Metastasis Rev 2006;25:387–408. [PubMed: 17043764]
40. Kolb R, Phan L, Borcherding N, Liu Y, Yuan F, Janowski AM, et al. Obesity-associated NLRC4 inflammasome activation drives breast cancer progression. Nat Commun 2016;7:13007. [PubMed: 27708283]
41. Pan D, Jiang C, Ma Z, Blonska M, You MJ, Lin X. MALT1 is required for EGFR-induced NF-kappaB activation and contributes to EGFR-driven lung cancer progression. Oncogene 2016;35:919–28. [PubMed: 25982276]
42. Pan D, Zhu Y, Zhou Z, Wang T, You H, Jiang C, et al. The CBM Complex Underwrites NF-kappaB Activation to Promote HER2-Associated Tumor Malignancy. Mol Cancer Res 2016;14:93–102. [PubMed: 26392569]

43. Fontan L, Yang C, Kabaleeswaran V, Volpon L, Osborne MJ, Beltran E, et al. MALT1 small molecule inhibitors specifically suppress ABC-DLBCL in vitro and in vivo. Cancer Cell 2012;22:812–24. [PubMed: 23238016]

44. Nagel D, Spranger S, Vincendeau M, Grau M, Raffegerst S, Kloo B, et al. Pharmacologic inhibition of MALT1 protease by phenothiazines as a therapeutic approach for the treatment of aggressive ABC-DLBCL. Cancer Cell 2012;22:825–37. [PubMed: 23238017]

45. Fontan L, Melnick A. Molecular pathways: targeting MALT1 paracaspase activity in lymphoma. Clin Cancer Res 2013;19:6662–8. [PubMed: 24004675]

46. Bertossi A, Krappmann D. MALT1 protease: equilibrating immunity versus tolerance. EMBO J 2014;33:2740–2. [PubMed: 25361604]

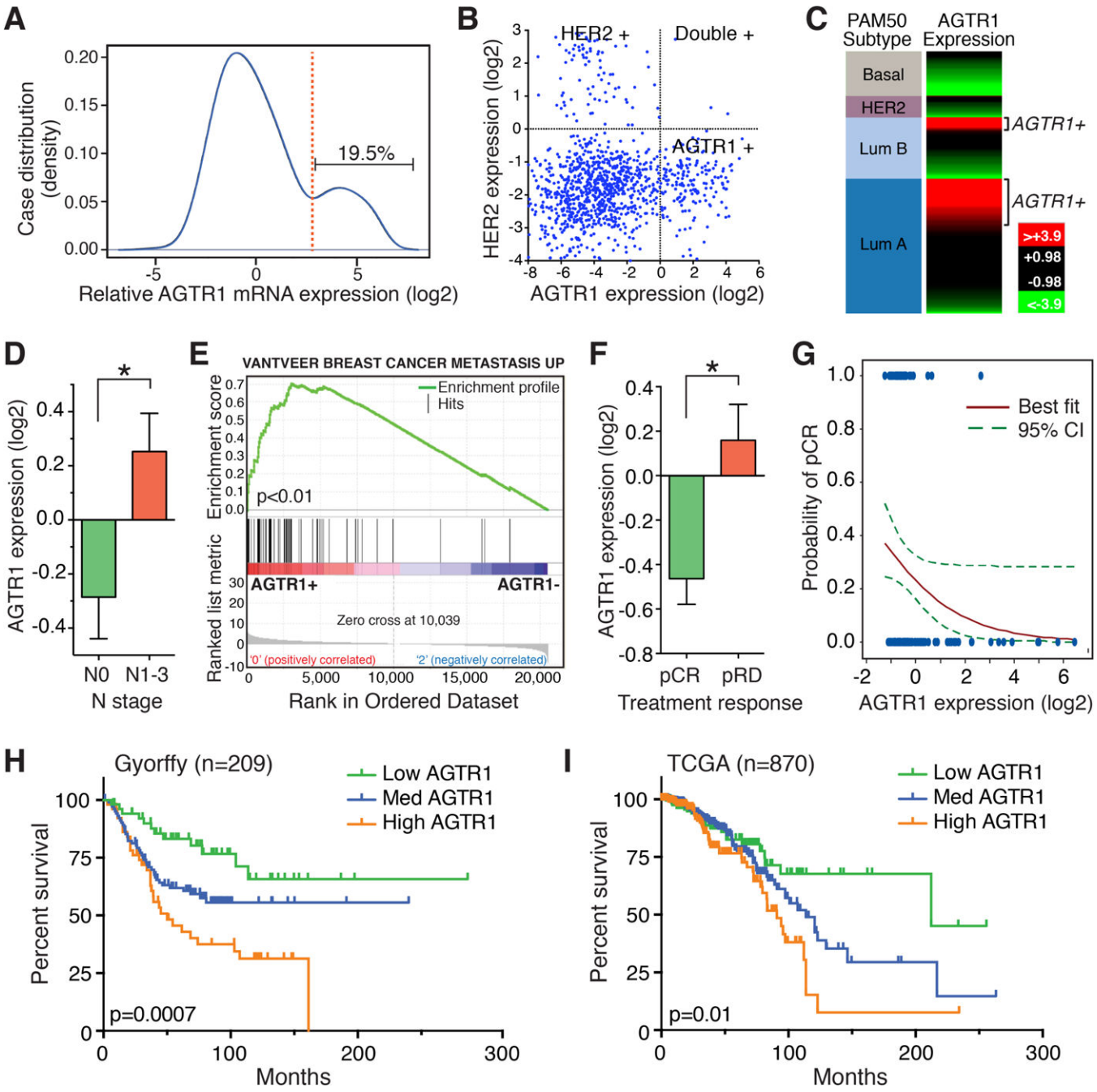

Figure 1. AGTR1 is expressed in a subset of breast cancers and is associated with aggressive disease.

A, kernel density plot analysis for AGTR1 mRNA expression in TCGA invasive breast cancer, based on Agilent microarray v1 data (n=526). **B,** scatter plot of HER2 and AGTR1 mRNA expression in the same TCGA cases. **C,** heatmap subcategorization of AGTR1+ cases in luminal A and B categories based on PAM50 subtype analysis (n=1094, scale: log2 mean centered). **D,** AGTR1 expression as a function of N stage (nodal status) for invasive ductal carcinoma, based on TCGA data (n=756; *, p=0.01). **E,** GSEA performed on AGTR1-stratified breast cancers in the TCGA collection using the

"VANTVEER_BREAST_CANCER_METASTASIS_UP" gene set. **F,** AGTR1 mRNA expression as a function of response to neoadjuvant chemotherapy. Patients undergoing 24 weeks of preoperative therapy with paclitaxel and fluorouracil-doxorubicin-cyclophosphamide (T/FAC) were analyzed for pathologic response at the time of subsequent surgery (pCR, pathologic complete response; pRD, pathologic residual disease; n=133; *, p=0.01). **G,** data from panel F are used to construct a pCR probability curve based on AGTR1 expression. Blue dots represent individual patients with either pCR or pRD. **H** and **I**, Kaplan-Meier survival curves based on AGTR1 expression (quartiles). Panel H shows outcomes (relapse-free survival; RFS) for patients with high-grade ER+, luminal B tumors in the Gyorffy meta-analysis and panel I shows outcomes (overall survival; OS) for ductal cancers in the TCGA dataset. P values generated by the Mantel-Cox test are indicated.

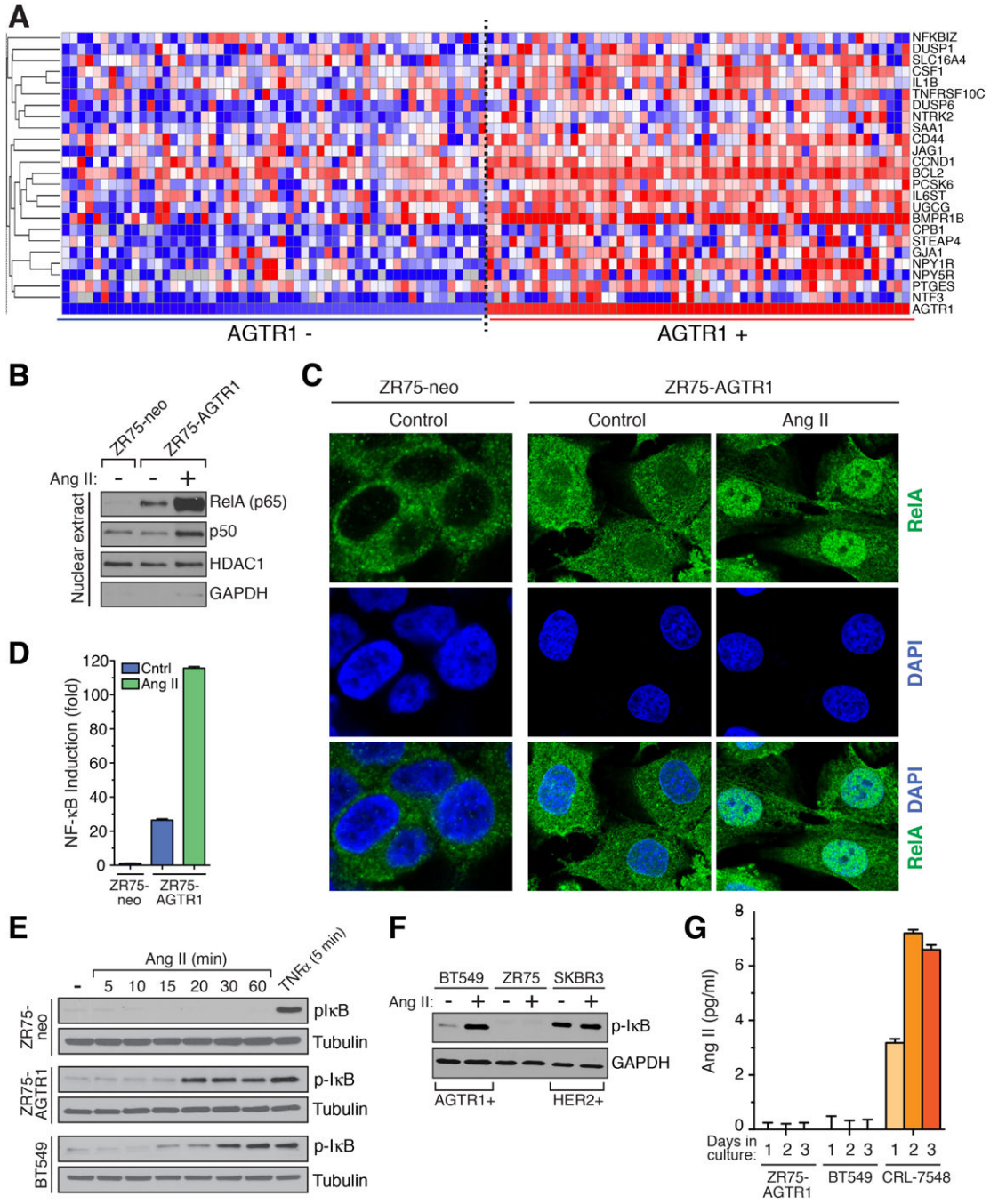

Figure 2. AGTR1 drives NF-κB activity in breast cancer.

A, heatmap of expression (high=red, low=blue) for key NF-κB regulated genes in luminal A/B breast cancer cases with the highest versus lowest AGTR1 expression (top/bottom 10% from TCGA dataset). **B** and **C**, nuclear translocation of NF-κB subunits (RelA and p50) in AGTR1-expressing ZR75 cells, ± 1 hr Ang II, as assessed by Western analysis of nuclear fractions (B), and by immunofluorescence (C). Nuclear extract integrity is demonstrated by the presence of nuclear protein, HDAC1, and the absence of contaminating cytoplasmic protein, GAPDH. **D**, NF-κB luciferase reporter activity in ZR75-derived lines ± Ang II

(mean ± SEM, n=3). **E**, Ang II-dependent NF-κB activation in AGTR1+ cells, as measured by Western blot for p-IkB. TNFa is used as a positive control. **F**, NF-κB activity in BT549 cells as compared to the HER2+, SKBR3 line. **G**, Ang II levels, as measured by ELISA, within media taken from the culture of the indicated cell lines (mean ± SD, n=3).

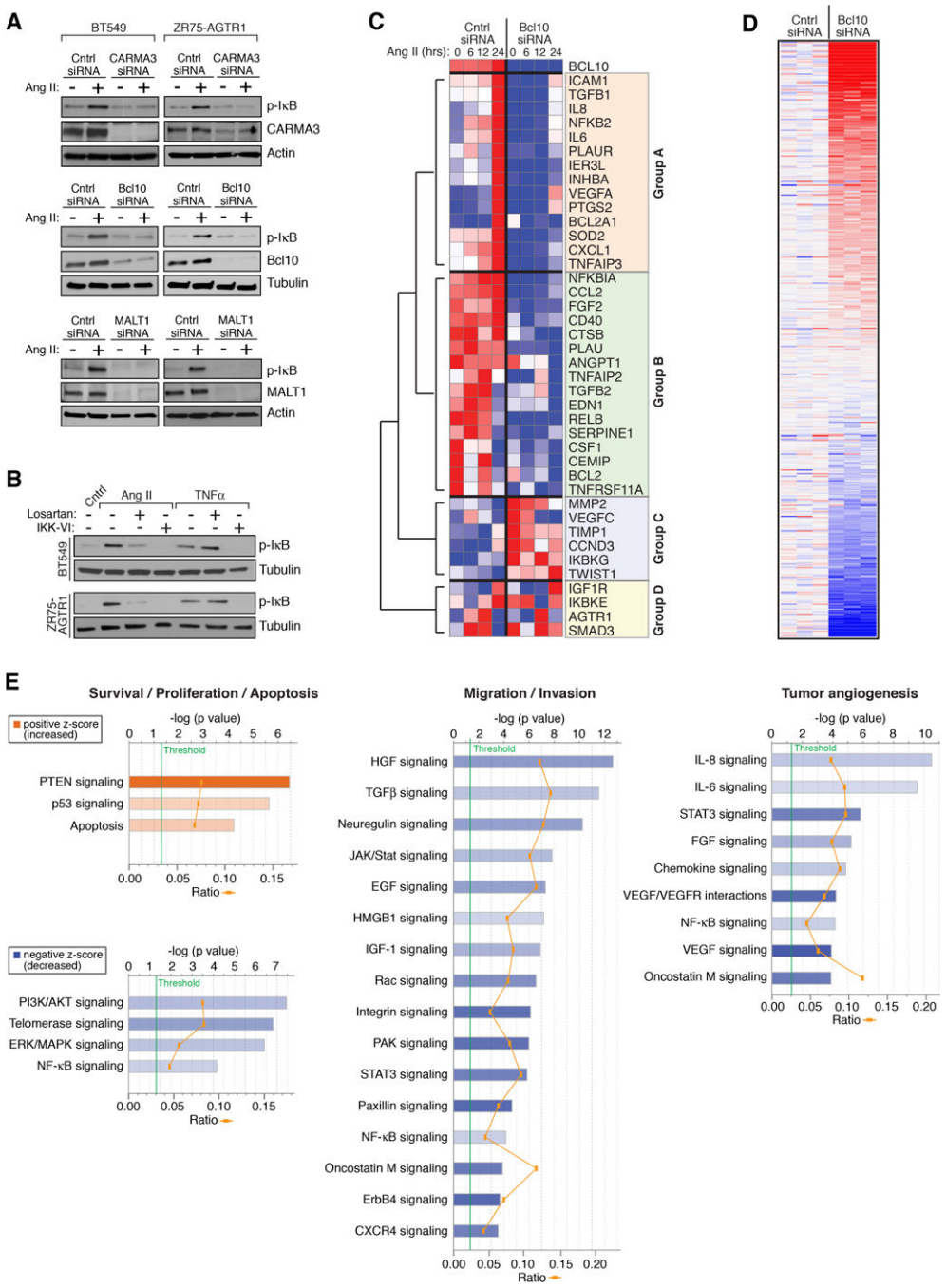

Figure 3. The CBM signalosome mediates NF-κB activation and gene expression reprogramming in AGTR1+ breast cancer.

A, effect of siRNA-mediated knockdown of each individual component of the CBM signalosome on Ang II-dependent NF-κB activation in either BT549 or ZR75-AGTR1 cells. **B**, effect of losartan (5 μM) or IKK-VI (5 μM) on Ang II-dependent NF-κB activation in AGTR1+ breast cancer lines. As expected, the response to TNFα is blocked only by IKK-VI and not losartan. **C**, siRNA-mediated Bcl0 knockdown in BT549 cells and effect on NF-κB gene targets. **D**, heatmap of gene expression changes in BT549 cells following Bcl10

knockdown by siRNA, in biological triplicate (upregulated=red, downregulated=blue). Analysis includes 487 genes from the Nanostring Pancancer Progression codeset for which expression could be reliably determined. **E**, Ingenuity Pathway Analysis (IPA) based on data from panel (D). Bar graphs indicate level of significance of change in the indicated pathways (-log p value). Increasingly dark blue color indicates greater reduction in pathway activity, while increasingly dark orange color indicates greater enhancement.

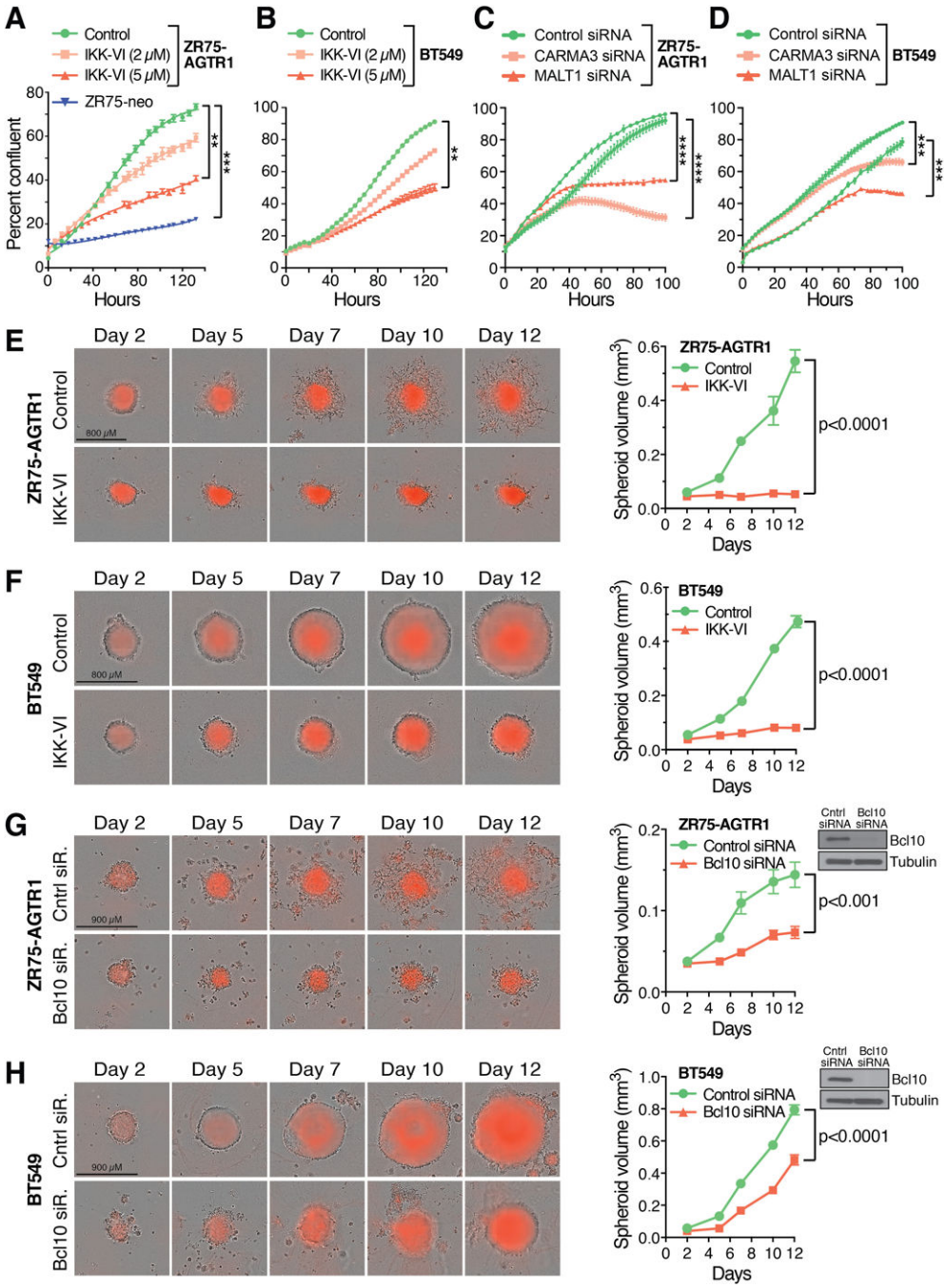

Figure 4. The CBM/NF-κB pathway is critical for AGTR1-dependent cell proliferation.

A and **B,** proliferation of ZR75-AGTR1 and BT549 cells in 2D, ± IKK-VI, as assessed using the quantitative IncuCyte system (mean ± SEM, n=4; **, p<0.01; ***, p<0.001). **C** and **D**, proliferation of the ZR75-AGTR1 and BT549 cell lines ± CARMA3 or MALT1 knockdown (mean SEM, n=3; ***, p<0.001; ****, p<0.0001). **E** and **F**, growth of ZR75-AGTR1 and BT549 spheroids ± IKK-VI (mean ± SEM, n=12). **G** and **H**, growth of ZR75-AGTR1 and BT549 spheroids ± Bcl10 knockdown (mean ± SEM, n=12).

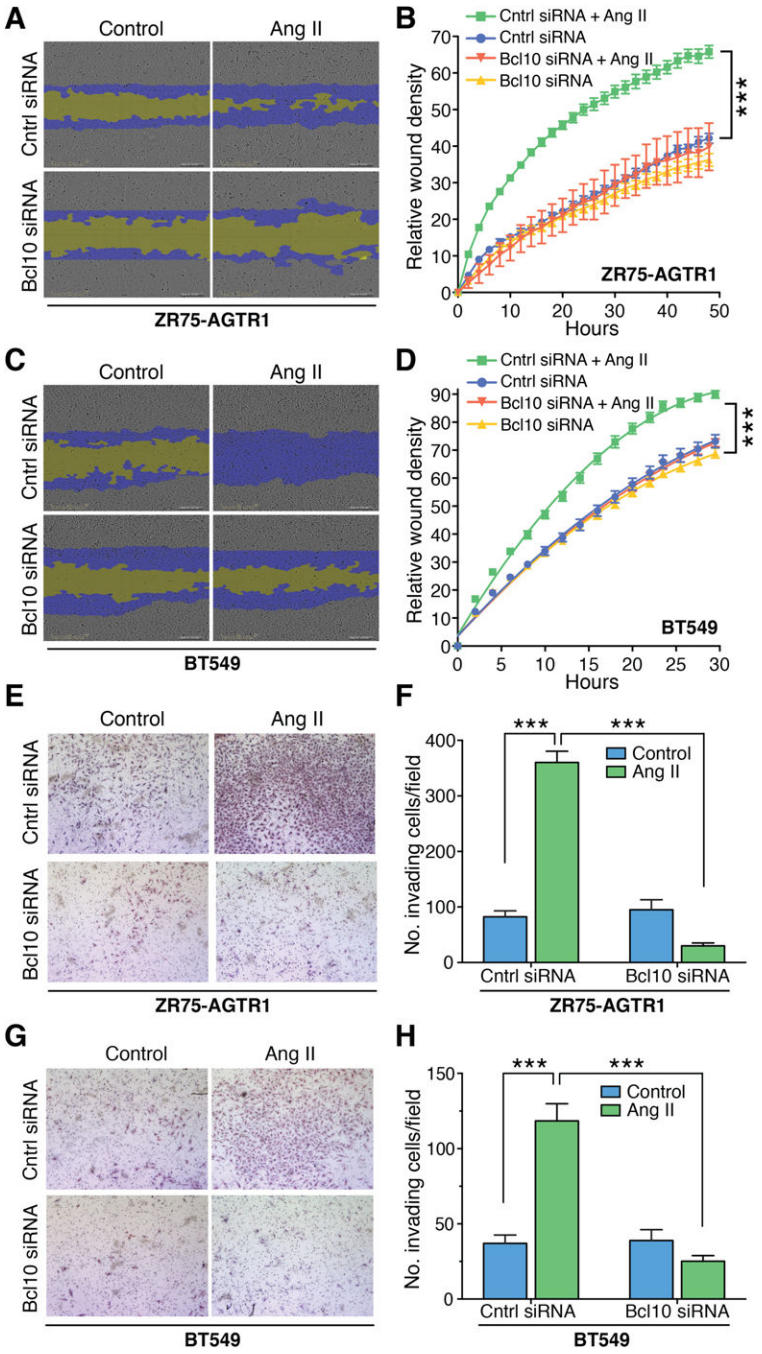

Figure 5. The CBM pathway is critical for Ang II-induced cell migration and invasion.

A and **B**, ZR75-AGTR1 cell migration was monitored in a real-time scratch assay, using the IncuCyte system. Representative scratch wounds are shown at the conclusion of the experiment. The region of the original scratch is pseudo-colored in yellow and the area of cell migration into the scratch is overlaid in blue/purple. Wound density (closure) is plotted as a continuous function of time (mean ± SEM, n=5; ***, $p<0.001$). **C** and **D**, BT549 cell migration was monitored as described for ZR75-AGTR1 cells (mean ± SEM, n=11; ***, $p<0.001$). **E** and **F**, ZR75-AGTR1 cell invasiveness as measured using matrigel-coated

Boyden chambers (mean ± SEM, n=3; ***, p<0.001). **G** and **H**, BT549 cell invasiveness as measured in Boyden chambers (mean ± SEM, n=3; ***, p<0.001).

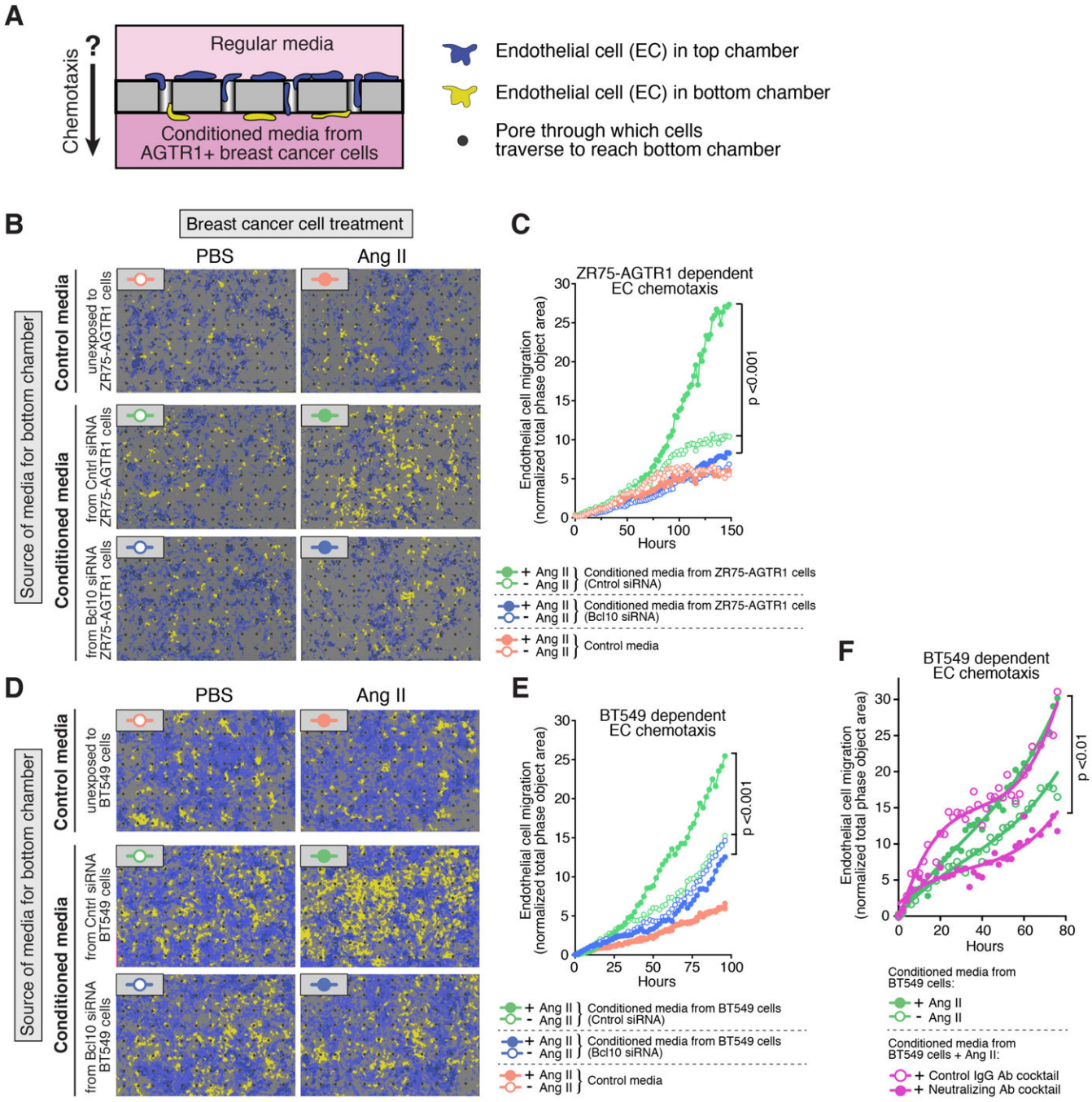

Figure 6. The CBM pathway is critical for paracrine-mediated chemotactic signaling to endothelial cells.

A, schematic of the IncuCyte-based, endothelial chemotaxis assay system. **B-E**, HUVEC endothelial cells were tested for chemotactic migration towards distinct sources of media placed in the bottom chamber. Representative static images showing both endothelial cells that completed migration (yellow) and those that did not (blue) at the conclusion of experiments are shown. Panels **C** and **E** show quantitative measures of endothelial chemotaxis as a continuous function of time, (n=4). **F**, effect of a cocktail of neutralizing

antibodies against IL-1β, IL-6, IL-8, SERPINE1 (PAI-1), VEGFA, and INHBA, on induced endothelial chemotaxis. Antibodies were incubated with conditioned media from Ang II-treated BT549 cells for 1 hr before proceeding to the chemotaxis assay. An isotype-matched control antibody cocktail was used as a negative control.

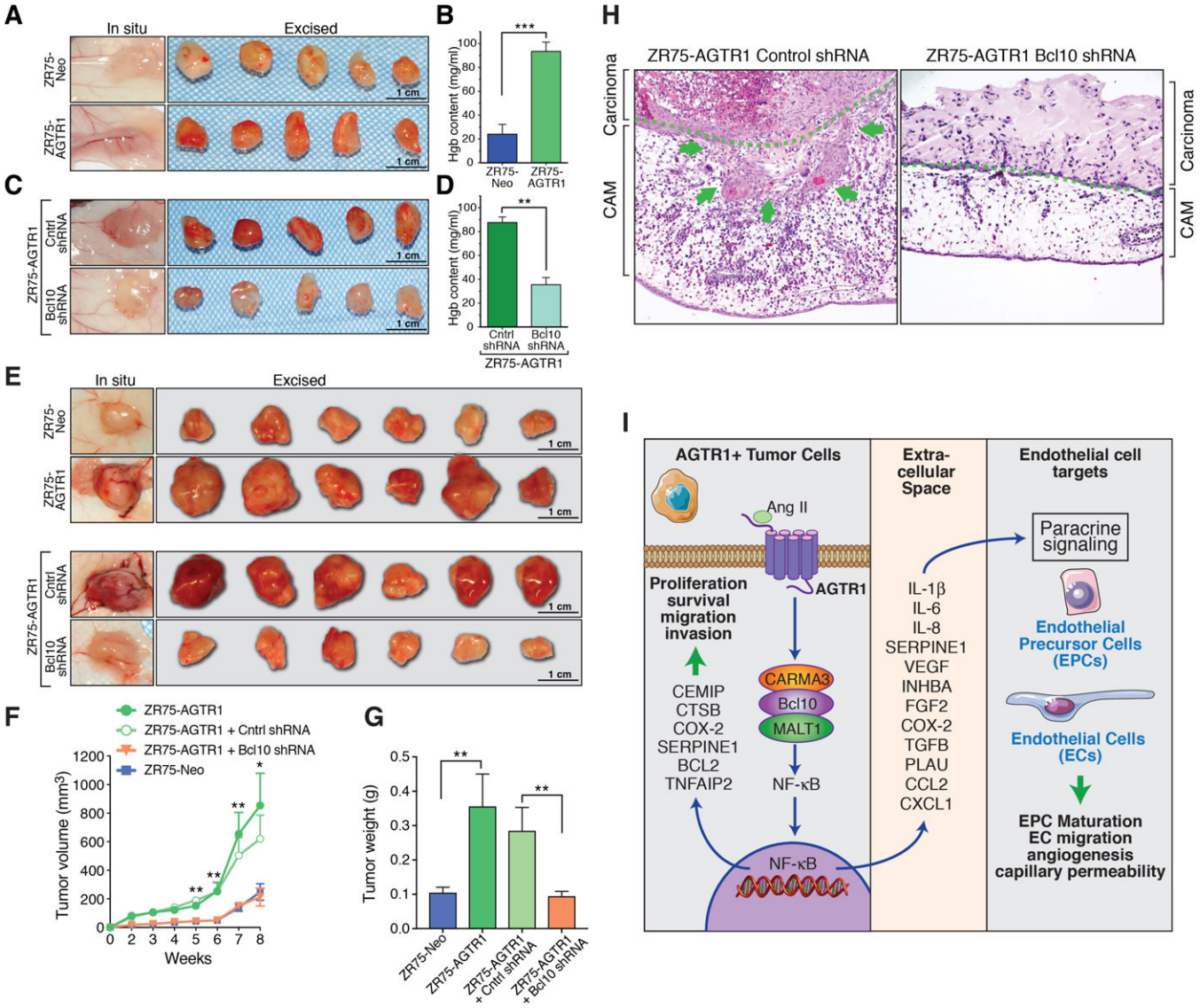

Figure 7. The CBM pathway is critical for tumor angiogenesis in vivo.

A and **B**, ZR75-AGTR1 cells were compared to control ZR75-neo cells for evidence of tumor-induced angiogenesis, using a subcutaneous angiogenesis plug assay in nude mice. Five representative excised plugs from each group (out of n=12/group) are shown. Panel **B** shows quantification of hemoglobin content of excised plugs (mean ± SEM, n=6; ***, $p<0.001$). **C** and **D**, plugs containing ZR75-AGTR1 cells with control versus Bcl10 knockdown. Plugs composed of Bcl10 knockdown cells were markedly pale relative to control counterparts and showed reduced hemoglobin content (mean ± SEM, n=6; **, $p<0.01$). **E-G**, enforced AGTR1 expression in ZR75 cells confers enhanced xenograft growth *in vivo*, which is fully abrogated by shRNA-mediated Bcl10 knockdown. Photos show the six largest xenografts from each group (out of n=10–12). Quantification of tumor volume and final weights are shown in panels **F** and **G** (mean ± SEM, n=10–12; **, $p<0.01$). Xenografts composed of cells expressing AGTR1 were also grossly more vascularized. Knockdown of Bcl10 strongly abrogated vascularization in addition to impairing tumor

growth. **H**, representative photomicrographs (200x) of CAMs after four days of exposure to ZR75-AGTR1 cancer cells (± Bcl10 knockdown), placed on the CAM surface (n=7). Green dotted line indicates the level of the CAM surface epithelium, representing the interface between the breast cancer cells and the underlying membrane. Green arrows highlight an area of disruption in the surface epithelium, with underlying tissue reaction. **I**, schematic summarizing both cancer cell intrinsic and extrinsic effects of AGTR1 overexpression in breast cancer that likely conspire to promote aggressive phenotype.